Biophysical Journal
Article

Biophysical Society

Ion-dependent DNA configuration in bacteriophage capsids

Pei Liu,[1] Javier Arsuaga,[2,3,*] M. Carme Calderer,[1] Dmitry Golovaty,[4,*] Mariel Vazquez,[2,5] and Shawn Walker[6]
[1]School of Mathematics, University of Minnesota, Twin Cities, Minneapolis, Minnesota; [2]Department of Mathematics and [3]Department of Molecular and Cellular Biology, University of California Davis, Davis, California; [4]Department of Mathematics, The University of Akron, Akron, Ohio; [5]Department of Microbiology and Molecular Genetics, University of California Davis, Davis, California; and [6]Department of Mathematics, Louisiana State University, Baton Rouge, Louisiana

ABSTRACT Bacteriophages densely pack their long double-stranded DNA genome inside a protein capsid. The conformation of the viral genome inside the capsid is consistent with a hexagonal liquid crystalline structure. Experiments have confirmed that the details of the hexagonal packing depend on the electrochemistry of the capsid and its environment. In this work, we propose a biophysical model that quantifies the relationship between DNA configurations inside bacteriophage capsids and the types and concentrations of ions present in a biological system. We introduce an expression for the free energy that combines the electrostatic energy with contributions from bending of individual segments of DNA and Lennard-Jones-type interactions between these segments. The equilibrium points of this energy solve a partial differential equation that defines the distributions of DNA and the ions inside the capsid. We develop a computational approach that allows us to simulate much larger systems than what is possible using the existing molecular-level methods. In particular, we are able to estimate bending and repulsion between the DNA segments as well as the full electrochemistry of the solution, both inside and outside of the capsid. The numerical results show good agreement with existing experiments and with molecular dynamics simulations for small capsids.

SIGNIFICANCE The spatial configuration of the viral genome inside the capsid is a key factor in determining the infectivity of the virus. We develop a continuum model of the double-stranded DNA genome inside an icosahedral protein capsid that allows us to simulate how the organization of the packaged genome is determined by the coupling of the mechanical properties of the DNA segments and the full electrochemistry of the electrolytes present inside and outside of the capsid. Our method facilitates the numerical description of much larger systems than currently possible using techniques that typically operate at a discrete molecular level.

INTRODUCTION

Bacteriophages are viruses that infect bacteria. Icosahedral double-stranded DNA bacteriophages pack their genome in a roughly spherical protein capsid. The length of the genome is on the order of tens of microns, whereas the diameter of the capsid is in the 10–50 nm range. The tightly packaged DNA molecule forms liquid crystal phases that have been observed and confirmed by both experimental and theoretical studies since the 1980s (1–10). The infectivity of bacteriophages, partly determined by the packing on their genome, has stimulated a number of potential applications, ranging from phage therapy (11) and drug discovery (12,13) to the food industry (14).

The structure and properties of the viral DNA inside protein capsids have been modeled using both continuum (15,16) and molecular simulations, including Monte Carlo (17–19), energy minimization (20), Brownian dynamics (21–25), Langevin dynamics (26), and molecular dynamics (27). These molecular-level methods are capable of predicting the trajectory of the viral genome and elucidating liquid crystalline properties (23). However, computational costs limit the size of a system that can be simulated to genomes that are only a few thousand basepairs in length.

In (28,29), we adopted the view that DNA packed inside the capsid is in a columnar hexagonal liquid crystalline state and that the equilibrium configuration of the system is determined in competition between DNA bending, electrostatic, and entropic effects (30). In (28), we used a continuum

Submitted November 20, 2020, and accepted for publication July 7, 2021.
*Correspondence: jarsuaga@ucdavis.edu or dmitry@uakron.edu
Editor: Christine Heitsch.
https://doi.org/10.1016/j.bpj.2021.07.006

mechanics model to study the liquid crystal structure of the encapsidated genome. This model is motivated by the data obtained with cryo-electron microscopy. The data suggest that DNA is in a disordered state in the middle of the capsid, whereas it forms an ordered structure in the vicinity of the capsid wall (5,31–34). The ordered region features locally parallel DNA segments that form a triangular lattice on a perpendicular cross section. In (28), the encapsidated DNA is characterized by a director—a unit vector representing the preferred local orientation of the DNA segments—and a scalar order parameter reflecting the degree of order of the DNA packing. This parameter can be assumed to be equal to 1 in the ordered region, whereas it equals 0 in the disordered region. The model incorporates three energy contributions for the entropic cost of the disordered region, the bending of the DNA molecule in the ordered region, and the DNA-DNA interactions. Numerical results show that the DNA segments wind around the axis of the capsid in the ordered region and predict the osmotic pressure inside the capsid, as well as the size of the disordered region. The DNA-DNA interaction term is a macromolecular model of the form introduced by de Gennes and Kleman (35,36) and by Oswald and Pieransky (37).

Because electrochemistry plays a significant role in the packing (38,39), folding (40,41), and ejection of the viral genome (31,42,43), here we build upon the methods in (28) to further characterize how ions affect DNA-DNA interactions in the ordered region of the genome, their distribution, and energetics inside the capsid.

The DNA chain is negatively charged, with a linear charge density of about 6e/nm, where e is the elementary charge. The aqueous environment with a high ionic concentration plays an essential role in screening the electrostatic repulsion between the DNA segments and neutralizing the overall charge distribution. Experiments and molecular simulations have shown that the encapsidated DNA structure is sensitive to, and can be controlled by, the ionic conditions (31,40,41,43,44). For example, single-molecule studies and molecular dynamics simulations show that high concentrations of positive ions may induce DNA condensation, significantly increasing the shear stresses of the DNA molecule and reducing the pressure inside the capsid (27,38). With increasing salt concentration and the resulting increase in concentrations of positive counterions, the spacing between two DNA segments reduces because both DNA self-repulsion and resistance to bending are weaker under these conditions (41).

Ions affect the DNA conformation inside the viral capsid according to two possible mechanisms. The first one is through mean-field electrostatic interactions, which account for basic DNA-DNA repulsion and can be described by the Poisson-Boltzmann theory (45). The second one is by changing the DNA persistence length. This goes beyond the mean-field description of the electrostatics and can be accounted for through the Debye-Hückel theory with charge renormalization (45,46). Various approximations have been proposed to model the dependence of the persistence length on the environmental ionic conditions. These include the Odijk-Skolnick-Fixman (OSF) model for high ionic conditions (47,48), the OSF-Manning formula that offers a correction to the OSF model for low ion concentrations (49), the Netz-Orland model that agrees with a wide range of experimental data using two fitting parameters (50), and an interpolation formula with four fitting parameters that works for the whole ionic strength range (51). Here, we use the OSF model because the goal of this work is to consider ionic solutions comparable to those found in experimental systems (41).

In addition to considering the electrostatic contributions, we use the Oseen-Frank energy to penalize the bending distortions of the hexagonal chromonic liquid crystal structure (29) and introduce the repulsive Lennard-Jones potential to account for the interaction between nearby DNA segments. The goal of this work is to provide a simple and efficient model that describes the connection between ionic effects and the DNA distribution in a bacteriophage capsid. The approach proposed here provides a fast alternative to molecular simulations that investigate the role of ionic conditions on packing of DNA in bacteriophage capsids. Indeed, for bacteriophages with long genomes, our model provides the only computationally feasible alternative that captures the qualitative features of an ionic state of a bacteriophage capsid and is capable of making quantitative predictions regarding the behavior of this system. A further advantage of our model is that any changes in the ionic conditions are automatically incorporated into the set of governing equations without any structural modifications to the model. Because of its consistent mathematical formulation, our framework is also amenable to incorporating additional effects, including attraction between DNA segments (25,52), the presence of multivalent ionic groups and condensing agents, and the degree of permeability of the capsid to different ionic species.

This work is organized as follows. The Materials and methods section presents the details of the analytical and computational model of the packaged DNA in the presence of ions. The Results and discussion section describes the outcomes of numerical simulations for a small "virtual" capsid and for the bacteriophage P4. Our observations are in qualitative agreement with previously published experimental and simulation results (27,41). In particular, we show that 1) the center region of the capsid cannot be occupied by ordered DNA segments because of a prohibitively large bending energy, 2) the DNA has ordered packing near the capsid wall with the repulsion between the DNA segments preventing the DNA density from being too large, 3) the presence of ions decreases variation of the DNA density in the ordered state, 4) the distance between nearby

DNA segments decreases with increasing ionic concentrations, and 5) as more DNA is packed into the capsid, the total energy of the system increases, and the packing process becomes more and more difficult.

MATERIALS AND METHODS

In this section, we focus on studying the local densities of ordered DNA basepairs and ions. We define the free energy of this multicomponent system by combining ideas from electrochemistry and the theory of nematic liquid crystals. Then, the equilibrium distributions of the DNA and ions can be determined by finding the minimizers of the free energy, which entails solving a set of nonlinear partial differential equations (PDEs).

Geometry of the viral capsid and encapsidated DNA

The bacteriophage capsid is a protein enclosure that typically has an icosahedral shape. For simplicity, we describe it as a rigid sphere of radius r_0,

$$\mathcal{B} = \left\{ (r,\theta,z) \middle| -r_0 \le z \le r_0, \right.$$

$$\left. 0 \le \theta < 2\pi, 0 \le r \le \sqrt{r_0^2 - z^2} \right\}, \quad (1)$$

where (r, θ, z) are cylindrical coordinates. We suppose that the unit vectors $\vec{e}_r$, $\vec{e}_\theta$, and $\vec{e}_z$ point in the directions of increasing r, θ, and z, respectively. As shown in Fig. 1 *a*, the DNA chain winds in the direction of $\vec{e}_\theta$, around the z axis, which is assumed to be perpendicular to the plane of the figure. It is worth mentioning that any shape of the capsid with axial symmetry can be treated in a similar way as described in the later sections.

To reduce the problem further, we postulate that the director field $\vec{n}$ is equal to the unit vector $\vec{e}_\theta$, which is shown to be a good approximation in (28). This allows us to assume that the entire system is rotationally symmetric so that all equations are independent of θ. The intersection of the DNA with the r-z plane is a hexagonal lattice, as illustrated in Fig. 1 *b*. The cross-sectional density is a function in space, denoted as $m_0(r, z)$. Thus, the concentration of DNA is $c_0(r, z) = \eta m_0(r, z)$, where η is a constant representing the line number density along the DNA chain. Here, we choose $\eta = 3\ \mathrm{nm}^{-1}$, corresponding to the rise of one basepair of DNA along the chain (i.e., about 0.34 nm) (53).

Note that we do not explicitly enforce connectivity of the DNA molecule in our model. From the energetic point of view, we assume that the energy of stretching of the DNA molecule along its axis to is negligible compared with that from other contributions. This has been shown to be true by molecular simulations by Petrov and Harvey (54). The information about the director field and the density of the DNA can be used to reconstruct a family of continuous curves representing possible configurations of a spooled DNA chain. Specifically, considering that the director field is tangent to the center curve of the DNA, the latter can be obtained by direct integration. Moreover, this framework also allows accounting for DNA stretching by relaxing the unit length constraint on the director field—a well-known procedure in liquid crystal modeling (55).

There are N ionic species in the system, whose valences and concentrations are denoted by z_i and $c_i(r, z)$ for $1 \le i \le N$, respectively. The exterior of the capsid containing ions is described as a large cylinder

$$\Omega = \{(r,\theta,z) | -L \le z \le L, 0 \le \theta < 2\pi, 0 \le r \le L\}, \quad (2)$$

with the height and the radius L, where $L > r_0$ so that the cylinder contains the capsid $\mathcal{B}$ in its interior.

Free energy of encapsidated DNA in the presence of ions

We define the total free energy of the system as follows:

$$E_{cap}[c_i(r,z)] = \int_{\mathcal{B}} k_3 \left| \vec{n} \times \nabla \times \vec{n} \right|^2 dx + \frac{1}{2} \int_{\Omega} \sum_{i=0}^{N} z_i e c_i \phi dx$$

$$+ k_B T \int_{\Omega} \left[\gamma c_0 \log c_0 + \sum_{i=1}^{N} c_i \log c_i \right] dx + \int_{\mathcal{B}} f(c_0) dx. \quad (3)$$

The first term comes from the Oseen-Frank free energy of liquid crystals, describing the bending energy of the DNA segments. Note that the energy corresponding to splay and twist vanishes because of $\vec{n} = \vec{e}_\theta$. The bending coefficient k_3 is proportional to the number density of the DNA segments and to the persistence length ℓ_p of DNA (15,25):

$$k_3 = k_B T \ell_p m_0. \quad (4)$$

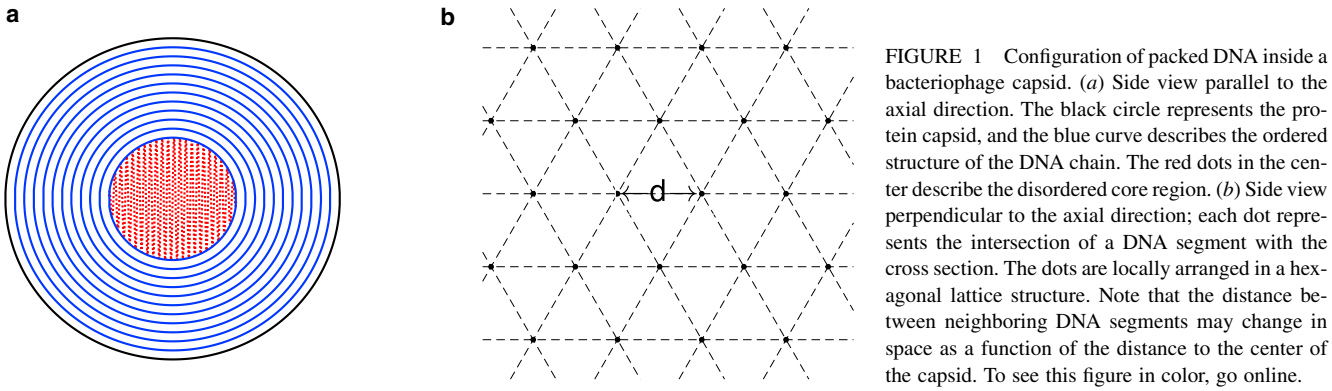

FIGURE 1 Configuration of packed DNA inside a bacteriophage capsid. (*a*) Side view parallel to the axial direction. The black circle represents the protein capsid, and the blue curve describes the ordered structure of the DNA chain. The red dots in the center describe the disordered core region. (*b*) Side view perpendicular to the axial direction; each dot represents the intersection of a DNA segment with the cross section. The dots are locally arranged in a hexagonal lattice structure. Note that the distance between neighboring DNA segments may change in space as a function of the distance to the center of the capsid. To see this figure in color, go online.

The dependence of the DNA persistence length ℓ_p on the ionic condition is modeled using the OSF theory,

$$\ell_p = \ell_0 + \frac{q^2}{16\pi\sum_{i=1}^{N} z_i^2 e^2 c_i}. \tag{5}$$

Here, e is the elementary charge, and qe is the DNA line charge density. The constant ℓ_0 represents the persistence length of the DNA when the ionic concentrations approach infinity. It can be obtained by fitting the experimental data (51).

The second term in Eq. Eq. 3 describes the electrostatic energy, where ϕ is the mean electrical potential, satisfying Poisson's equation:

$$-\epsilon\nabla^2\phi = \sum_{i=0}^{N} z_i e c_i. \tag{6}$$

The scalar ϵ represents the dielectric coefficient, and $z_0 = q/(\eta e)$ describes the valence of one DNA basepair. The boundary condition is Dirichlet $\phi = 0$ on $\partial\Omega$, which describes the overall charge neutrality in the large box Ω.

The third term in Eq. 3 captures the contribution from the entropy of DNA and all ionic species. Here, the entropic density of the two-dimensional hexagonal structure of DNA is proportional to $k_B T m_0(r,z)\log m_0(r,z)$, multiplied by the factor of $2\pi r$, where the cylindrical coordinate r is the radius of the DNA segment. This expression is equivalent to the DNA entropy in Eq. 3. It also contains a constant weight γ that accounts for the fact that DNA is a polymer, unlike the mobile ions. This is a typical assumption in the Flory-Huggins theory of polymers (56–58).

The fourth term in Eq. 3 describes the interaction between the DNA segments inside the capsid. Considering that the DNA chain is tightly packed, we use the standard 6-12 Lennard-Jones potential to represent the interactions between DNA segments. Ignoring the weak attraction, we model the repulsion between neighboring DNA segments by $f(c_0) \propto \frac{c_0}{d^{12}}$. Given the hexagonal lattice structure of DNA, the distance d satisfies $d^2 \propto \frac{1}{c_0}$. Thus, we set

$$f(c_0) = \alpha k_B T c_0^7, \tag{7}$$

where α is a coefficient controlling the strength of the repulsion. This energy accounts for the contribution from the elasticity of the system and prevents the DNA density from being unreasonably high. The attraction term in the Lennard-Jones potential could only have minor effects by slightly increasing the DNA density in the regions with low DNA concentration.

Now, the total energy simplifies to

$$E_{cap}[c_i(r,z)] = \int_{\mathcal{B}} \frac{k_3}{r^2} dx + \frac{1}{2}\int_{\Omega}\sum_{i=0}^{N} z_i e c_i \phi dx$$

$$+k_B T\int_{\Omega}\left[\gamma c_0 \log c_0 + \sum_{i=1}^{N} c_i \log c_i\right]dx + k_B T\int_{\mathcal{B}} \alpha c_0^7 dx. \tag{8}$$

Governing equations for the equilibrium distribution

In this section, we derive the set of partial differential equations governing the equilibrium distributions of DNA and ions both inside and outside of the capsid. The chemical potential of each species is obtained by computing the variation of the total energy (Eq. 8) with respect to the concentrations of that species. It follows that the concentrations of the DNA and the ions are given implicitly by a modified Boltzmann's distribution. They can now be determined with the help of the Poisson's equation, taking the form of a modified Poisson-Boltzmann equation.

We first calculate the chemical potential of DNA,

$$\mu_0 = \frac{\delta E_{cap}}{\delta c_0(r,z)} = z_0 e\phi + \gamma k_B T(\log c_0 + 1) + \chi\left(\frac{\ell_p}{\eta r^2} + 7\alpha c_0^6\right), \text{ in } \Omega, \tag{9}$$

where $\chi = 1$ in $\mathcal{B}$ and $\chi = 0$ in $\Omega/\mathcal{B}$. In equilibrium, the chemical potential of DNA must be constant in Ω and $\Omega/\mathcal{B}$, respectively, i.e.,

$$\mu_0 = \begin{cases} \mu_0^{b,in}, & \text{in } \Omega, \\ \mu_0^{b,out}, & \text{in } \Omega/\mathcal{B}. \end{cases} \tag{10}$$

Equation 10 describes the fact that the capsid $\mathcal{B}$ is not permeable to the DNA. Indeed, DNA can only be packaged inside or ejected from the capsid through the connector region. Modeling the packaging and ejection process is beyond the scope of this article. Here, $\mu_0^{b,in}$ and $\mu_0^{b,out}$ are two constants to be determined from the mass conservation of DNA,

$$\int_{\Omega} c_0 dx = N_0, \quad \int_{\mathcal{B}} c_0 dx = N_p. \tag{11}$$

N_0 is a number representing the total basepairs of DNA in the system, and N_p represents the number of DNA basepairs that is packaged in the capsid $\mathcal{B}$. Equations 9, 10, and 11 together implicitly determine the equilibrium distribution of the DNA, which can be viewed as a modified Boltzmann's distribution. Because equation Eq. 9 is highly nonlinear, an explicit form of the distribution is not expected.

Likewise, the chemical potentials of ions are

$$\mu_i = \frac{\delta E_{cap}}{\delta c_i(r,z)} = z_i e\phi + k_B T(\log c_i + 1) - \chi\frac{k_B T c_0 q^2 z_i^2}{16\pi\eta r^2\left(\sum_{i=1}^{N} z_i^2 e c_i\right)^2}, \text{ in } \Omega. \tag{12}$$

It should be noticed that the capsid $\mathcal{B}$ is permeable to the ions. At equilibrium, the chemical potential of each ionic species should be a constant in Ω,

$$\mu_i = \mu_i^b, \quad i = 1, 2, \ldots, N, \tag{13}$$

where μ_i^b is a constant to be determined from the mass conservation of the ith species,

$$\int_{\Omega} c_i dx = N_i. \tag{14}$$

Here, N_i describes the number of the ith ion in the system. Equations 12, 13, and 14 give the implicit distribution of ions.

Combining these distributions with Poisson's equation Eq. 6, we obtain a closed system of PDEs, which is in the form of a modified Poisson-Boltzmann's equation. Directly solving this system is a challenging task because of its high nonlinearity. Instead, we consider the following modified Poisson-Nernst-Planck equations, based on the gradient flow approach,

$$\begin{cases} -\epsilon\nabla^2\phi = \sum_{i=0}^{N} z_i e c_i, \\ \frac{\partial}{\partial t}c_i = \nabla\cdot J_i = \nabla\cdot\left(k_B T\nabla c_i + c_i\nabla\left(z_i e\phi - \frac{\chi k_B T c_0 q^2 z_i^2}{16\pi\eta r^2\left(\sum_{i=1}^{N} z_i^2 e c_i\right)^2}\right)\right), \ i = 1,2,\cdots,N, \\ \frac{\partial}{\partial t}c_0 = \nabla\cdot J_0 = \nabla\cdot\left(k_B T\gamma\nabla c_0 + c_0\nabla\left(z_0 e\phi + \chi\frac{k_B T\ell_p}{\eta r^2}\right)\right). \end{cases} \tag{15}$$

The boundary conditions on $\partial\Omega$ are

$$\begin{cases} \phi = 0, \\ J_i\cdot\vec{e}_n = 0, \ i = 0,1,\cdots,N. \end{cases} \tag{16}$$

The interface conditions on $\partial\mathcal{B}$ are

$$\begin{cases} [\phi] = 0, \\ \left[\epsilon\nabla\phi\cdot\vec{e}_n\right] = 0, \\ [\mu_i] = 0, \ i = 1,2,\cdots,N, \\ \left[J_i\cdot\vec{e}_n\right] = 0, \ i = 1,2,\cdots,N, \\ J_0\cdot\vec{e}_n = 0. \end{cases} \tag{17}$$

Here, $[\cdot]$ represents the jump of a given quantity across the capsid wall and $\vec{e}_n$ is the unit normal vector of the interface $\partial\mathcal{B}$. It is straightforward to verify that this system satisfies the following equation, implying that the energy is decreasing in time:

$$\frac{d}{dt}E_{cap} = -\int_{\Omega}\sum_{i=0}^{N}\frac{J_i^2}{c_i}dx. \tag{18}$$

When $t\to\infty$, the solution of Eq. 15 approaches the equilibrium described by Eqs. 9, 10, 11, 12, and 13. We developed an efficient numerical method for solving the convection-diffusion system Eq. 15. The details of the numerical algorithm are summarized in the Supporting materials and methods.

Estimation of the radial probability distribution of DNA and ions

We define the average of the density $c_i(r)$ on a sphere of radius r as

$$\rho_i(r) = \frac{\int_0^{\pi}\int_0^{2\pi} c_i(r,\theta,\phi)\sin\phi d\theta d\phi}{\int_0^{\pi}\int_0^{2\pi}\sin\phi d\theta d\phi}. \tag{19}$$

Similarly, the radial probability distribution is defined as

$$P_i(r) = \frac{\int_0^{\pi}\int_0^{2\pi} c_i(r,\theta,\phi)r^2\sin\phi d\theta d\phi}{\int_{\Omega} c_i(r,\theta,\phi)r^2\sin\phi dr d\theta d\phi}. \tag{20}$$

Here, (r, θ, ϕ) correspond to the spherical coordinates, and $r^2\sin\phi$ is the Jacobian used to convert from Cartesian to spherical coordinates. The radial probability distribution describes the probability of finding one DNA segment on a sphere of radius r centered at the origin (27). It is related to the structure factor obtained in experiments such as those that use x-ray or neutron scattering techniques.

Estimation of the distance between the DNA segments

The distance d between parallel DNA segments is now estimated using the hexagonal lattice structure with known density c_0:

$$\frac{\sqrt{3}}{2}d^2\times\frac{c_0}{\eta} = 1. \tag{21}$$

Here, $\frac{\sqrt{3}}{2}d^2$ represents the area of a hexagon of diameter d, and $\frac{c_0}{\eta} = m_0$ is the cross-sectional density. So,

$$d = \sqrt{\frac{2\eta}{\sqrt{3}c_0}}. \tag{22}$$

RESULTS AND DISCUSSION

In this section, we present the numerical results obtained by solving equation Eq. 15 for particular bacteriophages. The parameters are chosen based on the real biological systems. Here, $\eta = 3\ \mathrm{nm}^{-1}$, describing the fact that one basepair of DNA corresponds to about 0.34 nm of length along the DNA axis (53). The line charge density is approximately $q = 6e/\mathrm{nm}$ (59), so that $z_0 = \frac{q}{\eta e} = 2$. The dielectric coefficient is set to be that of water at room temperature, i.e., $\epsilon = 78$. We select the parameters α and γ so that the contributions from the corresponding terms to the total energy Eq. 8 have comparable values. This choice assumes that different physical effects incorporated into our model have non-negligible influence on the overall behavior of the system. In the following, we set $\gamma = 0.33$.

We first apply our model to a virtual bacteriophage, which was simulated in (27). The viral capsid has a radius $r_0 = 12.5$ nm and genome length $N_0 = 3000$ bp. To consider the equilibrium state, we assume that all the DNA is inside the capsid; thus, $N_p = N_0$. The average concentration of DNA is $c_a = 3N_0/(4\pi r_0^3) \approx 0.37$ nm^{-3}. We set $\alpha = 0.4^{-7}$ nm[21]. There are two ionic species, Na^+ (or Mg^{2+}) and Cl^-, in the system. The overall charge neutrality requires

$$z_0N_0 + z_1N_1 + z_2N_2 = 0. \quad (23)$$

All numerical simulations are performed in a large cylinder $\Omega = \{(r, \theta, z) | -25 \le z \le 25, 0 \le \theta < 2\pi, 0 \le r \le 25\}$. We suppose that the system is invariant with respect to rotations around the z axis and reflections with respect to the xy plane so that all concentration and potential fields satisfy $g(r, \theta, z) = g(r, -z) = g(r, z)$. It follows that we only need to solve the system of governing equations in the first quadrant of the r-z plane. The region exterior to Ω is considered to be vacuum, and all concentrations in that region will be set equal to zero, which is consistent with the molecular simulations in (27). Note that the simulation box in (27) is rectangular.

Density distribution of DNA and ions inside viral capsids

Fig. 2 shows a quadrant of the DNA density (*left pane*) and the ionic densities for Na^+ (*middle*) and Cl^- (*right*) in the r-z plane. Here, the bulk concentration of NaCl is set to be 100 mM. The DNA density outside of the capsid is identically zero because we assume that the DNA is completely packaged. Additionally, there is a core region close to the central axis of the capsid (the *z axis* in the figure) where the DNA density is negligible. The radius of this region is about 2 nm and indicates that the DNA molecule cannot be perfectly ordered at the center region of the capsid because of its bending rigidity. Further away from the center, the DNA density increases, showing that DNA tends to stay close to the capsid, mainly because of the effects of the DNA bending energy. The contribution from the Lennard-Jones repulsion prevents the DNA from condensing at the capsid and instead forces the DNA density to be nearly homogeneous in the region outside the inner core. Interestingly, the figure also shows a sharp transition zone between the inner core and the outer region.

The distribution of Na^+ is shown in Fig. 2 *b*. Na^+ follows the distribution of DNA because the negatively charged DNA attracts (or absorbs) positive charges. Because the capsid is permeable to ions, outside of the capsid the Na^+ density is very small (though not zero). As expected, the distribution of Cl^- behaves in an opposite manner (Fig. 2 *c*). Cl^- ions are repelled from the region where the DNA is located and displaced to the inner core region and to the region outside of the capsid.

In conclusion, our results show that inside the capsid NaCl dissociates into its positive and negative ions. Positive ions mostly associate with the DNA molecule, whereas negative ions are expelled to the center of the capsid (where DNA is mostly absent) and to the region outside the capsid.

Estimation of the radial probability distribution of DNA and ions

Next, we compute the average of the density $c_i(r)$ on a sphere of radius r, as explained in the Materials and methods section. Fig. 3 shows the results for three different concentrations of NaCl. To better visualize the curves, we renormalized the densities as follows:

$$\overline{\rho}_i(r) = \rho_i(r) \Big/ \int_0^{25} \rho_i(r)dr$$

With an increasing salt concentration, we observe a lower maximum of the DNA density curve (this maximum occurs near the protein capsid). As expected, at the same time, the ion concentration increases both inside and outside of the viral capsid.

To compare our results with those previously obtained in molecular simulations, we also calculated the radial probability distribution of the DNA and the ions. Fig. 4 shows the probability distributions for DNA (*black*), Na^+ (*red*), and Cl^- (*blue*).

The probability distributions of DNA inside the capsid increases monotonically with the distance from the center

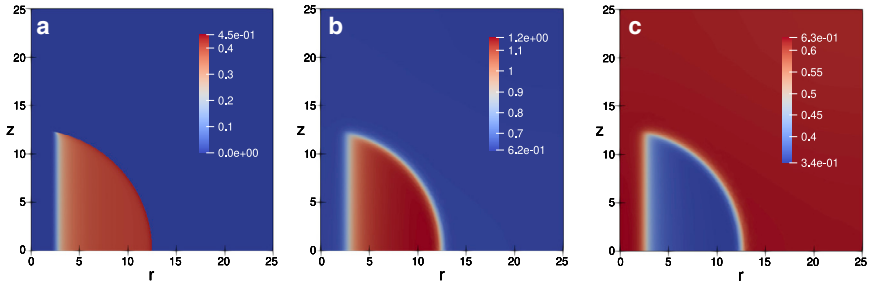

FIGURE 2 Number density (nm^{-3}) in the r-z plane. (*a*) DNA, (*b*) Na^+, and (*c*) Cl^-. To see this figure in color, go online.

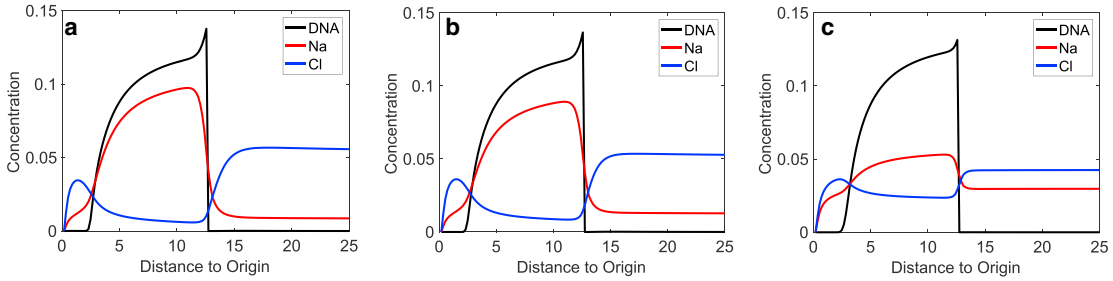

FIGURE 3 Average radial distribution $\overline{\rho}_i(r)$ under different ionic conditions. (*a*) 100 mM NaCl, (*b*) 166 mM NaCl, and (*c*) 1 M Na Cl. All the curves are renormalized and dimensionless. To see this figure in color, go online.

core, mirroring the increase of the DNA density. Our results are in agreement with those reported in (27), with a small difference in the DNA distribution. The probability distributions for ions are consistent with those presented in Fig. 2 *a* and clearly show the colocalization of positive ions with the DNA and of positive and negative ions. When the distance to the origin is larger than $L = 25$, the integration of Eq. 20 is conducted in part over the exterior region of Ω, where the concentrations are set to zero. This explains why the probabilities approach zero when the distance to the origin is large.

We also note that Fig. 4 shows only one local maximum of the DNA probability distribution next to the protein capsid, whereas the results in (27) identify two discrete layers of DNA. This difference is because, in our model, the DNA double helix is not described explicitly; instead, its discrete structure is implicitly given by the averaged DNA concentration. This is a known limitation of the Poisson-Boltzmann theory that arises from neglecting steric effects in dense electrolytes. Improvements to the model can be made by introducing steric energy in the modified Poisson-Boltzmann theory, resulting in a model that better resolves the discrete DNA chain. This extension of the Poisson-Boltzmann approach will inevitably introduce extra complexity into the model and is beyond the scope of this work.

Next, we performed a numerical experiment in which we oversaturated the sample with 1.6 M NaCl (Fig. 4 *b*). We observe that the Na^+ and Cl^- curves apparently overlap, contrary to what is seen in the other two panels. This could be understood from Fig. 3. We note that, as the overall concentration of NaCl increases, the concentration of Cl^- in the region enclosed by the capsid increases faster than in the capsid exterior, whereas the average concentration of Na^+ in the region enclosed by the capsid increases more slowly than in the capsid exterior. The combination of these two events produces two similar curves.

Spacing between the DNA segments as a function of the ionic concentration

We investigated the average separation between the DNA segments as a function of the salt concentration. It has been observed that as the concentration of positive ions increases, the average distance between the DNA segments decreases, in both molecular simulation (27) and experiment (41).

Fig. 5 describes the distance between the DNA segments under different ionic conditions. Because the value of c_0, and therefore d, is a function of the spatial location, we computed their values at two different cross-sectional locations. In Fig. 5, the curve labeled (11, 0) corresponds to the DNA spacing near the protein capsid, and the curve labeled (7, 0) corresponds to DNA spacing halfway between the center and the protein capsid. Both curves show that the distance between the DNA segments decreases with higher salt concentrations. The main reason is because the persistence length is monotonically decreasing with ionic strength, facilitating the packing of DNA into an ordered hexagonal structure. This result is in agreement with the experimental observations reported in (27,41).

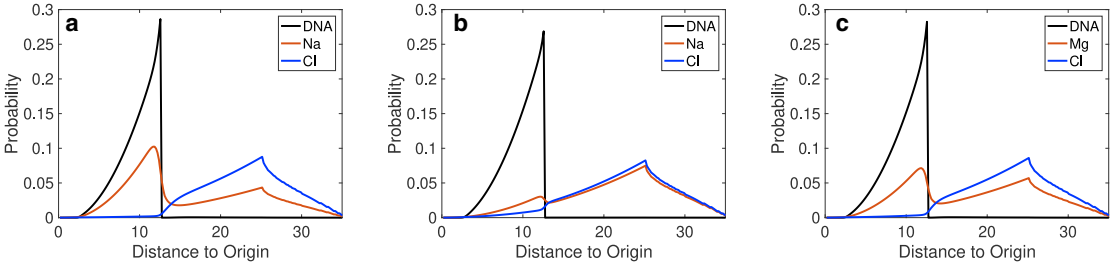

FIGURE 4 Probability distributions for DNA (*black*), Na^+ (*red*), and Cl^- (*blue*) under different ionic conditions. (*a*) 100 mM NaCl, (*b*) 1 M NaCl, and (*c*) 100 mM $MgCl_2$. To see this figure in color, go online.

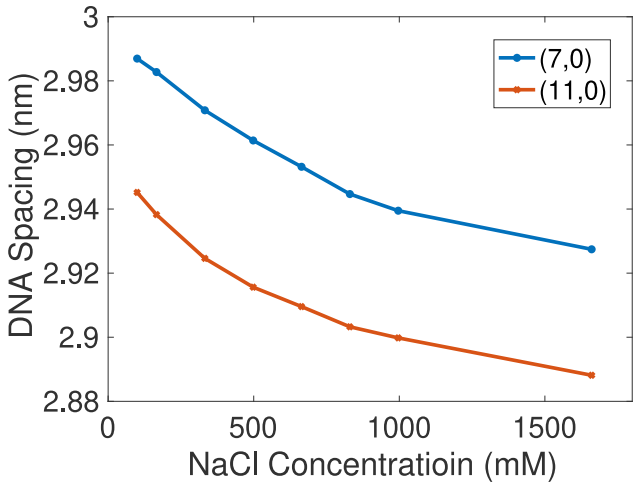

FIGURE 5 Distance between the DNA segments as a function of NaCl concentration at cross-sectional locations (11, 0) and (7, 0) in a capsid with radius $r_0 = 12.5$ nm centered at the origin. To see this figure in color, go online.

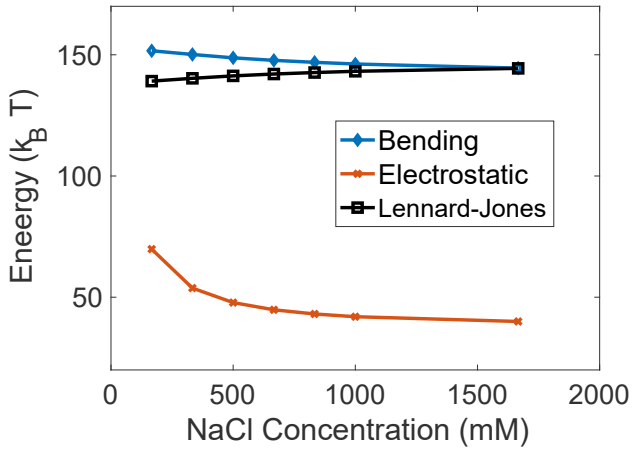

FIGURE 6 The energy from bending, electrostatic, and Lennard-Jones for increasing NaCl concentrations. To see this figure in color, go online.

Estimation of the bending, electrostatics, and Lennard-Jones contributions to the total energy of the system

As discussed earlier, ionic concentrations affect both the shielding of negative charges along the DNA molecule and the persistence length of DNA. To better understand the origin of the observed difference in the DNA segments separation as a function of ionic concentration, we investigated the contribution of the different components of the energy to the total energy.

Fig. 6 shows the contribution of the electrostatic, bending, and Lennard-Jones energies to the total energy of the system. Although the bending and Lennard-Jones energies are larger in value than the electrostatic energy, they are weakly dependent on the ionic concentrations, whereas electrostatic is more sensitive. As the salt concentration increases, the overall bending energy and electrostatic energy decrease and the Lennard-Jones potential increases slightly. The decrease in electrostatic energy is due to the screening in the electrical potential; the decrease in bending energy is explained because of the decrease in persistence length, and therefore, the Lennard-Jones energy increases because of the smaller distance between the DNA segments.

Simulations for P4 phage

The genome of bacteriophage P4 is 11.5 kb, and, being a satellite of bacteriophage P2, all of its structural proteins are encoded by P2. The P4 capsid has icosahedral symmetry (T = 4) and is 45 nm in diameter (60). Therefore, we set the radius of the capsid $r_0 = 22.5$ nm and the genome length $N_0 = 11.5$ kb with $N_p = N_0$, i.e., the entire DNA is inside the capsid. The average concentration of DNA is $c_a = 3N_0/(4\pi r_0^3) = 0.24$ nm^{-3}. We set $\alpha = 0.2^{-7}$ nm^{21}.

The behavior of the density distributions of DNA and ions is similar to Fig. 2. The core region at the center of the capsid has no (ordered) DNA, which has a radius of about 2 nm. Fig. 7 describes the distance between the DNA segments under different ionic conditions for P4 phages. Because the average concentration of DNA is smaller than the virtual bacteriophage discussed before, the distance between the nearby DNA segments in P4 phage is larger. Numerical results again show that the increasing ionic concentration causes the decreasing in the DNA spacing, which suggests that this observation is true for a variety of bacteriophages unless additional phenomena are considered.

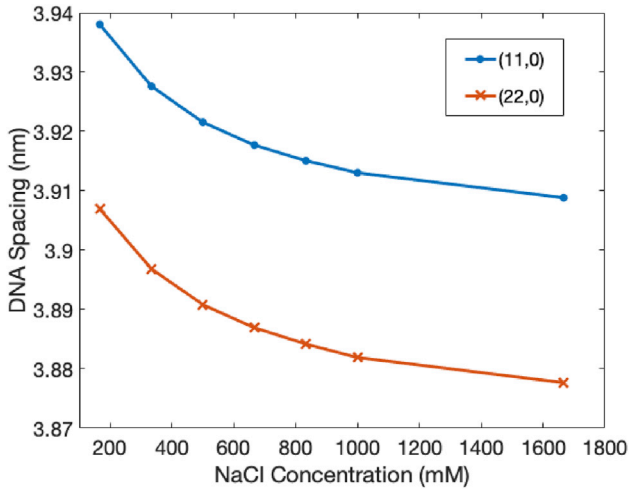

FIGURE 7 Distance between the DNA segments as a function of NaCl concentration at cross-sectional locations (22, 0) and (11, 0) in a capsid with radius $r_0 = 22.5$ nm centered at the origin. To see this figure in color, go online.

Estimation of the energy value as function of the DNA inside the capsid

Our approach can also be applied to study the packing process by varying the length of DNA N_p (in basepairs) packed inside of the capsid. Fig. 8 shows the total energy of the system at equilibrium, assuming different levels of DNA packing. Here, the radius is $r_0 = 22.5$ nm and the total genome length is $N_0 = 11{,}500$ bp. The bulk concentration of NaCl is 100 mM. The rest of the DNA is assumed to remain mobile in the region outside the capsid. The total energy increases with more packed DNA corresponding to the minimal energy required to overcome the pressure difference across the volume enclosed by the capsid, not including the friction forces. The concavity of the curve also indicates that the packing process becomes more and more difficult as more DNA is packed. This is consistent with the molecular simulation results of P4 phages (61). We also notice that the changes of energy at different levels of packing in our calculation are on the same order of magnitude as the repulsive region described in (61), which confirms that our choices of parameters are reasonable.

CONCLUSIONS

Ions are essential in multiple biological processes. In bacteriophages, ionic concentrations have been shown to play a key role in packaging (38,39), folding (41,62), and delivery (40) of the viral genome. In this work, we take a continuum approach to quantitatively describe the role played by ions in the folding of DNA inside the phage capsid.

Our approach expands on our previous work, in which we introduced a novel, to our knowledge, chromonic liquid crystal model for DNA inside a bacteriophage capsid (28,29). This model is designed based on pioneering continuum mechanics work by Tzlil et al. (25), as well as on the concept of a director introduced by Klug and Ortiz (15). However, the model in (28) implemented a phenomenological formulation of DNA-DNA interactions inspired by the works of de Gennes and Kleman (35,36) and by Oswald and Pieransky (37) that is not amenable to a detailed description of ionic interactions in the environment. To address this issue, we propose a model that explicitly introduces the ionic concentrations, their diffusion, and their interaction with the DNA molecule.

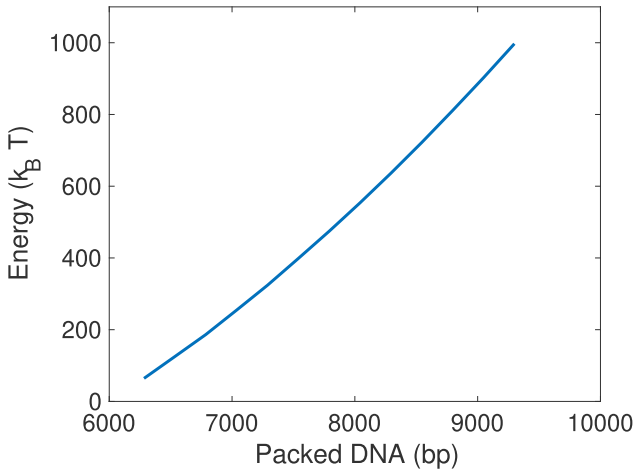

FIGURE 8 Total energy of the system with different amounts N_p (in basepairs) of DNA packed inside of the capsid. To see this figure in color, go online.

The proposed ionic model describes the distribution of ions both inside and outside the bacteriophage capsid and the average structure of the DNA packaged inside capsids. The model combines the Oseen-Frank energy from liquid crystal theory with salt-dependent persistence length, the electrostatic potential energy between charges, and the Lennard-Jones interaction potential between the DNA segments. A key aspect of our model is that it incorporates effects of the ionic conditions on the DNA-DNA interaction and their role in modulating the persistence length of the DNA molecule.

Our results are in agreement with those presented by Cordoba and colleagues (27). The model predicts the distribution of ions relative to the DNA molecule, and the distribution of DNA inside the capsid. We find that positive ions colocalize with the DNA molecule at relatively low ionic concentrations (but not diluted as found in common standard phage buffers), whereas negative ions are displaced either to the center core of the capsid, where DNA is mostly absent because of the high bending required to fill this volume, or outside of the capsid. The DNA-DNA interactions at this ionic concentration are mostly repulsive (61). Therefore, a higher concentration of DNA is found in very close proximity to the capsid. At saturated ionic concentrations, our model predicts a displacement of the DNA away from the capsid and an overall ionic saturation of the capsid and surrounding environment.

The model also captures the contribution of the different energy terms to the total energy of the system and how the ionic conditions affect this contribution. In (54), it was reported that both electrostatic and entropic effects account for most of the energy of the system. Here, we find that the bending energy and the Lennard-Jones potential also play an important role. Our results are in agreement with experimental results obtained by Qui et al. (41).

Based on the agreement of our results with known DNA and ionic distribution inside the viral capsid, the distance between the DNA segments, and the energies, we conclude that the model presented in this work can capture the structure of the packaged phage DNA under experimental conditions. Also, as a continuum model, solving the equations numerically is much faster compared with the approaches based on molecular simulations and can be applied to large bacteriophages.

Several improvements to this model can be considered. We described the charges mainly within the framework of

the Poisson-Boltzmann theory, which has limitations because of the omission of the correlation effects (63,64). In our model, the structure of the DNA segments is implicitly given by the averaged concentrations. To capture the discrete layer structure, as was done in (27,61), we need to add in the pairwise correlation energy from the hard-sphere repulsion. The OSF theory for modeling the ion-dependent persistence length while effectively accounting for the electrostatic correlations proved to be successful with high ionic concentrations. Possible extensions to lower ionic concentrations can be made by employing other theories. Our approach can also be extended to study the packing dynamics by considering the length of DNA packed inside of the capsid to be time dependent, with proper interface conditions at the capsid itself.

Experiments (9) and molecular dynamics simulations (54) have shown that the addition of polyvalent cations introduces attractive effects between the DNA segments and promotes the formation of toroidal structures (65). This suggests promising avenues for future research.

SUPPORTING MATERIAL

Supporting material can be found online at https://doi.org/10.1016/j.bpj.2021.07.006.

AUTHOR CONTRIBUTIONS

J.A., M.C.C., and M.V. designed the research. M.C.C., D.G., P.L., and S.W. formulated the model. P.L. and S.W. developed and implemented the numerical method. P.L. carried out all simulations and analyzed the data. All authors participated in writing of the article.

ACKNOWLEDGMENTS

This work was partially supported by National Science Foundation grants DMS-1817156 (J.A. and M.V.), DMS-1816740 (M.C.C. and P.L.), DMS-1729538 (D.G.), and DMS-1555222-CAREER (S.W.).

SUPPORTING CITATIONS

Reference (66) can be found in the Supporting material.

REFERENCES

1. Lepault, J., J. Dubochet, …, E. Kellenberger. 1987. Organization of double-stranded DNA in bacteriophages: a study by cryo-electron microscopy of vitrified samples. *EMBO J.* 6:1507–1512.
2. Kellenberger, E., E. Carlemalm, …, G. De Haller. 1986. Considerations on the condensation and the degree of compactness in non-eukaryotic DNA-containing plasmas. *In* Bacterial Chromatin. C. O. Gualerzi and C. L. Pon, eds. Springer, pp. 11–25.
3. Rill, R. L. 1986. Liquid crystalline phases in concentrated aqueous solutions of Na+ DNA. *Proc. Natl. Acad. Sci. USA.* 83:342–346.
4. Strzelecka, T. E., M. W. Davidson, and R. L. Rill. 1988. Multiple liquid crystal phases of DNA at high concentrations. *Nature.* 331:457–460.
5. Livolant, F. 1991. Ordered phases of DNA in vivo and in vitro. *Physica A.* 176:117–137.
6. Leforestier, A., and F. Livolant. 1993. Supramolecular ordering of DNA in the cholesteric liquid crystalline phase: an ultrastructural study. *Biophys. J.* 65:56–72.
7. Park, H.-S., S.-W. Kang, …, O. D. Lavrentovich. 2008. Self-assembly of lyotropic chromonic liquid crystal Sunset Yellow and effects of ionic additives. *J. Phys. Chem. B.* 112:16307–16319.
8. Leforestier, A., S. Brasilès, …, F. Livolant. 2008. Bacteriophage T5 DNA ejection under pressure. *J. Mol. Biol.* 384:730–739.
9. Leforestier, A., and F. Livolant. 2009. Structure of toroidal DNA collapsed inside the phage capsid. *Proc. Natl. Acad. Sci. USA.* 106:9157–9162.
10. Reith, D., P. Cifra, …, P. Virnau. 2012. Effective stiffening of DNA due to nematic ordering causes DNA molecules packed in phage capsids to preferentially form torus knots. *Nucleic Acids Res.* 40:5129–5137.
11. Doss, J., K. Culbertson, …, N. Barekzi. 2017. A review of phage therapy against bacterial pathogens of aquatic and terrestrial organisms. *Viruses.* 9:50.
12. Liu, J., M. Dehbi, …, M. DuBow. 2004. Antimicrobial drug discovery through bacteriophage genomics. *Nat. Biotechnol.* 22:185–191.
13. O'Sullivan, L., C. Buttimer, …, A. Coffey. 2016. Bacteriophage-based tools: recent advances and novel applications. *F1000 Res.* 5:2782.
14. Endersen, L., J. O'Mahony, …, A. Coffey. 2014. Phage therapy in the food industry. *Annu. Rev. Food Sci. Technol.* 5:327–349.
15. Klug, W., and M. Ortiz. 2003. A director-field model of DNA packaging in viral capsids. *J. Mech. Phys. Solids.* 51:1815–1847.
16. Purohit, P. K., J. Kondev, and R. Phillips. 2003. Mechanics of DNA packaging in viruses. *Proc. Natl. Acad. Sci. USA.* 100:3173–3178.
17. Arsuaga, J., M. Vazquez, …, J. Roca. 2005. DNA knots reveal a chiral organization of DNA in phage capsids. *Proc. Natl. Acad. Sci. USA.* 102:9165–9169.
18. Arsuaga, J., and Y. Diao. 2008. DNA knotting in spooling like conformations in bacteriophages. *Comput. Math. Methods Med.* 9:303–316.
19. Comolli, L. R., A. J. Spakowitz, …, K. H. Downing. 2008. Three-dimensional architecture of the bacteriophage φ29 packaged genome and elucidation of its packaging process. *Virology.* 371:267–277.
20. Arsuaga, J., R. K.-Z. Tan, …, S. C. Harvey. 2002. Investigation of viral DNA packaging using molecular mechanics models. *Biophys. Chem.* 101–102:475–484.
21. Harvey, S. C., A. S. Petrov, …, M. B. Boz. 2009. Viral assembly: a molecular modeling perspective. *Phys. Chem. Chem. Phys.* 11:10553–10564.
22. Spakowitz, A. J., and Z.-G. Wang. 2005. DNA packaging in bacteriophage: is twist important? *Biophys. J.* 88:3912–3923.
23. Marenduzzo, D., E. Orlandini, …, C. Micheletti. 2009. DNA-DNA interactions in bacteriophage capsids are responsible for the observed DNA knotting. *Proc. Natl. Acad. Sci. USA.* 106:22269–22274.
24. Cruz, B., Z. Zhu, …, M. Vazquez. 2020. Quantitative study of the chiral organization of the phage genome induced by the packaging motor. *Biophys. J.* 118:2103–2116.
25. Tzlil, S., J. T. Kindt, …, A. Ben-Shaul. 2003. Forces and pressures in DNA packaging and release from viral capsids. *Biophys. J.* 84:1616–1627.
26. Forrey, C., and M. Muthukumar. 2006. Langevin dynamics simulations of genome packing in bacteriophage. *Biophys. J.* 91:25–41.
27. Córdoba, A., D. M. Hinckley, …, J. J. de Pablo. 2017. A molecular view of the dynamics of dsDNA packing inside viral capsids in the presence of ions. *Biophys. J.* 112:1302–1315.
28. Walker, S., J. Arsuaga, …, M. Vázquez. 2020. Fine structure of viral dsDNA encapsidation. *Phys. Rev. E.* 101:022703.
29. Hiltner, L., M. C. Calderer, …, M. Vázquez. 2021. Chromonic liquid crystals and packing configurations of bacteriophage viruses. *Philos. Trans. A Math. Phys. Eng. Sci.* 379:20200111.
30. Riemer, S. C., and V. A. Bloomfield. 1978. Packaging of DNA in bacteriophage heads: some considerations on energetics. *Biopolymers.* 17:785–794.

31. Li, D., T. Liu, …, A. Evilevitch. 2015. Ionic switch controls the DNA state in phage λ. *Nucleic Acids Res.* 43:6348–6358.
32. Chang, J., P. Weigele, …, W. Jiang. 2006. Cryo-EM asymmetric reconstruction of bacteriophage P22 reveals organization of its DNA packaging and infecting machinery. *Structure.* 14:1073–1082.
33. Cerritelli, M. E., N. Cheng, …, A. C. Steven. 1997. Encapsidated conformation of bacteriophage T7 DNA. *Cell.* 91:271–280.
34. Lander, G. C., L. Tang, …, J. E. Johnson. 2006. The structure of an infectious P22 virion shows the signal for headful DNA packaging. *Science.* 312:1791–1795.
35. Gennes, P. D., J. Prost, and R. Pelcovits. 1995. The physics of liquid crystals. *Phys. Today.* 48:67.
36. Kleman, M. 1980. Developable domains in hexagonal liquid crystals. *J. Phys. (Paris).* 41:737–745.
37. Oswald, P., and P. Pieranski. 2005. Smectic and Columnar Liquid Crystals: Concepts and Physical Properties Illustrated by Experiments. CRC Press, Boca Raton, FL.
38. Keller, N., D. delToro, …, D. E. Smith. 2014. Repulsive DNA-DNA interactions accelerate viral DNA packaging in phage Phi29. *Phys. Rev. Lett.* 112:248101.
39. Keller, N., S. Grimes, …, D. E. Smith. 2016. Single DNA molecule jamming and history-dependent dynamics during motor-driven viral packaging. *Nat. Phys.* 12:757–761.
40. Evilevitch, A., L. T. Fang, …, C. M. Knobler. 2008. Effects of salt concentrations and bending energy on the extent of ejection of phage genomes. *Biophys. J.* 94:1110–1120.
41. Qiu, X., D. C. Rau, …, W. M. Gelbart. 2011. Salt-dependent DNA-DNA spacings in intact bacteriophage λ reflect relative importance of DNA self-repulsion and bending energies. *Phys. Rev. Lett.* 106:028102.
42. Evilevitch, A., L. Lavelle, …, W. M. Gelbart. 2003. Osmotic pressure inhibition of DNA ejection from phage. *Proc. Natl. Acad. Sci. USA.* 100:9292–9295.
43. Wu, D., D. Van Valen, …, R. Phillips. 2010. Ion-dependent dynamics of DNA ejections for bacteriophage λ. *Biophys. J.* 99:1101–1109.
44. Jin, Y., C. M. Knobler, and W. M. Gelbart. 2015. Controlling the extent of viral genome release by a combination of osmotic stress and polyvalent cations. *Phys. Rev. E Stat. Nonlin. Soft Matter Phys.* 92:022708.
45. Vlachy, V. 1999. Ionic effects beyond Poisson-Boltzmann theory. *Annu. Rev. Phys. Chem.* 50:145–165.
46. Alexander, S., P. Chaikin, …, D. Hone. 1984. Charge renormalization, osmotic pressure, and bulk modulus of colloidal crystals: theory. *J. Chem. Phys.* 80:5776–5781.
47. Odijk, T. 1977. Polyelectrolytes near the rod limit. *J. Polym. Sci. Polym. Phys. Ed.* 15:477–483.
48. Skolnick, J., and M. Fixman. 1977. Electrostatic persistence length of a wormlike polyelectrolyte. *Macromolecules.* 10:944–948.
49. Manning, G. S. 1981. A procedure for extracting persistence lengths from light-scattering data on intermediate molecular weight DNA. *Biopolymers.* 20:1751–1755.
50. Netz, R. R., and H. Orland. 2003. Variational charge renormalization in charged systems. *Eur. Phys. J. E Soft Matter.* 11:301–311.
51. Brunet, A., C. Tardin, …, M. Manghi. 2015. Dependence of DNA persistence length on ionic strength of solutions with monovalent and divalent salts: a joint theory–experiment study. *Macromolecules.* 48:3641–3652.
52. Luan, B., and A. Aksimentiev. 2008. DNA attraction in monovalent and divalent electrolytes. *J. Am. Chem. Soc.* 130:15754–15755.
53. Heath, G. R., M. Li, …, L. J. Jeuken. 2016. Layer-by-layer assembly of supported lipid bilayer poly-l-lysine multilayers. *Biomacromolecules.* 17:324–335.
54. Petrov, A. S., and S. C. Harvey. 2008. Packaging double-helical DNA into viral capsids: structures, forces, and energetics. *Biophys. J.* 95:497–502.
55. Lin, F.-H., and C. Liu. 1995. Nonparabolic dissipative systems modeling the flow of liquid crystals. *Commun. Pure Appl. Math.* 48:501–537.
56. de Gennes, P.-G. 1979. Scaling Concepts in Polymer Physics. Cornell University Press, Ithaca, NY.
57. Motoyama, M., H. Nakazawa, …, M. Aizawa. 2000. Phase separation of liquid crystal–polymer mixtures. *Comput. Theor. Polym. Sci.* 10:287–297.
58. Matsuyama, A., and R. Hirashima. 2008. Phase separations in liquid crystal-colloid mixtures. *J. Chem. Phys.* 128:044907.
59. Gilbert, R. 2009. Physical biology of the cell, by Rob Phillips, Jane Kondev and Julie Theriot. *Crystallogr. Rev.* 15:285–285.
60. Shore, D., G. Dehò, …, R. Goldstein. 1978. Determination of capsid size by satellite bacteriophage P4. *Proc. Natl. Acad. Sci. USA.* 75:400–404.
61. Petrov, A. S., and S. C. Harvey. 2011. Role of DNA-DNA interactions on the structure and thermodynamics of bacteriophages Lambda and P4. *J. Struct. Biol.* 174:137–146.
62. Evilevitch, A., W. H. Roos, …, G. J. Wuite. 2011. Effects of salts on internal DNA pressure and mechanical properties of phage capsids. *J. Mol. Biol.* 405:18–23.
63. Levin, Y. 2002. Electrostatic correlations: from plasma to biology. *Rep. Prog. Phys.* 65:1577–1632.
64. Parsegian, V. A., R. P. Rand, and D. C. Rau. 2000. Osmotic stress, crowding, preferential hydration, and binding: a comparison of perspectives. *Proc. Natl. Acad. Sci. USA.* 97:3987–3992.
65. Hud, N. V., and I. D. Vilfan. 2005. Toroidal DNA condensates: unraveling the fine structure and the role of nucleation in determining size. *Annu. Rev. Biophys. Biomol. Struct.* 34:295–318.
66. Rathgeber, F., D. A. Ham, …, P. H. Kelly. 2016. Firedrake: automating the finite element method by composing abstractions. *ACM Transactions on Mathematical Software*:43–24.